



CAMD 6-m toroidal grating monochromator beamline

K.D. Koch^a, Ch.V. Mohan^a, J.L. Erskine^{a,*}, P.T. Sprunger^b, J.D. Scott^b

^aDepartment of Physics, University of Texas at Austin, Austin, TX 78712-1081, USA

^bThe Bennett Johnson, Sr, Center for Advanced Microstructures and Devices, Louisiana State University, Baton Rouge, LA 70806, USA

Received 7 April 2001; received in revised form 5 July 2001; accepted 9 July 2001

Abstract

The design and performance of a 6-m 20° deflection-angle toroidal grating monochromator (TGM) installed on the 1.5 GeV CAMD electron storage ring is described. A novel front-end optical configuration based on float-glass mirror technology enables effective use of 28 mrad of bending magnet radiation. Ray tracing is used to evaluate and optimize the theoretical resolution and transmission of the TGM. Experiments that characterize the CAMD bending magnet source parameters and evaluate the performance of the float-glass mirror are described. Alignment procedures and measurements that establish beamline performance (resolution and flux) are presented. The CAMD TGM covers 10–200 eV, delivers good flux at moderate resolution ($\sim 2 \times 10^{12}$ photons/s in a 0.1% bandwidth) and achieves an ultimate resolving power of 2000. © 2002 Elsevier Science B.V. All rights reserved.

1. Introduction

In 1996, the University of Texas 6-m toroidal grating monochromator (TGM) was relocated from the National Synchrotron Light Source (NSLS) at Brookhaven National Laboratory, to the Center for Advanced Microstructures and Devices (CAMD) in Baton Rouge, Louisiana. The (conventional) TGM optical configuration at NSLS consisted of a 5° incidence-angle toroidal entrance mirror, a set of three Jobin Yvon (JY) 6-m 10° gratings [1] and a 5° ellipsoidal refocus mirror. The exit slit was mounted on a carriage permitting it to be translated to the optimum diffracted beam focus position as wavelength was scanned (thus reducing loss of resolution from vertical defocussing of the grating) [2–4]. Ray-

tracing studies [2] of the monochromator, based on holographic parameters for the grating set supplied by JY, yielded an optimum entrance mirror design and a table of optimum exit slit distances.

Adapting the TGM to the CAMD storage ring required a new approach to the monochromator input optics which has resulted in replacing the single toroidal mirror with a combination of three mirrors including a long cylindrical mirror based on commercial float-glass. This novel approach permits effective use of 28 mrad of bending magnet radiation.

2. Constraints, requirements and construction details

A primary design constraint was to preserve as much of the original optics and hardware as

*Corresponding author. Tel.: +1-512-471-1464.

E-mail address: erskine@physics.utexas.edu (J.L. Erskine).

possible. The CAMD electron storage ring typically operates at 1.5 GeV/170 mA (or 1.3 GeV/250 mA) and produces comparable flux to the NSLS 0.75 GeV/800 mA storage ring over the TGM operating range (20–200 eV) but considerably higher flux in the hard X-ray range. The heat load on the first optical element at 1.5 GeV/170 mA is sufficiently high (~ 90 W total) to require some type of cooling; in addition, the hard X-rays from the CAMD ring require more extensive radiation shielding than was required at NSLS which constrains the geometry of the front-end optics.

Space restrictions and other constraints imposed by radiation shielding and the need to eventually service a second beamline from a single 70 mrad bending magnet port rendered it physically impossible to effectively couple the source to the monochromator using the traditional approach based on a single ellipsoidal or toroidal mirror. In order to permit fine adjustments of the entrance slit and the vertical focus mirror without using stepper motors, a decision was made to locate these components outside the radiation shield wall.

This requirement placed the (entrance slit) vertical focus at about 11.5 m from the source. Various combinations of plane, spherical and cylindrical mirrors were considered to couple the bending magnet radiation into the existing TGM optics. Most configurations suffered from at least one problem such as an impractically large (and expensive) optical element, limited collection efficiency (poor use of the allocated 35 mrad) or a poor image at the slit resulting from aberrations. One configuration consisting of a plane mirror, a large cylindrical mirror and a reasonable size spherical mirror satisfied all of the constraints.

Fig. 1 illustrates the optical configuration of the CAMD 6-m TGM and the plan view only of the proposed spherical grating monochromator (SGM) beamline. Suitable separation ($\sim 14^\circ$) of the two beamlines is achieved by using large horizontal collection mirrors that accept nearly 30 mrad of bending magnet radiation and direct the focused radiation along axes that diverge from the front-end mirror tank. Table 1 presents the principal parameters of the 6-m TGM optical elements. The mirrors M_1 and M_2 are housed in a

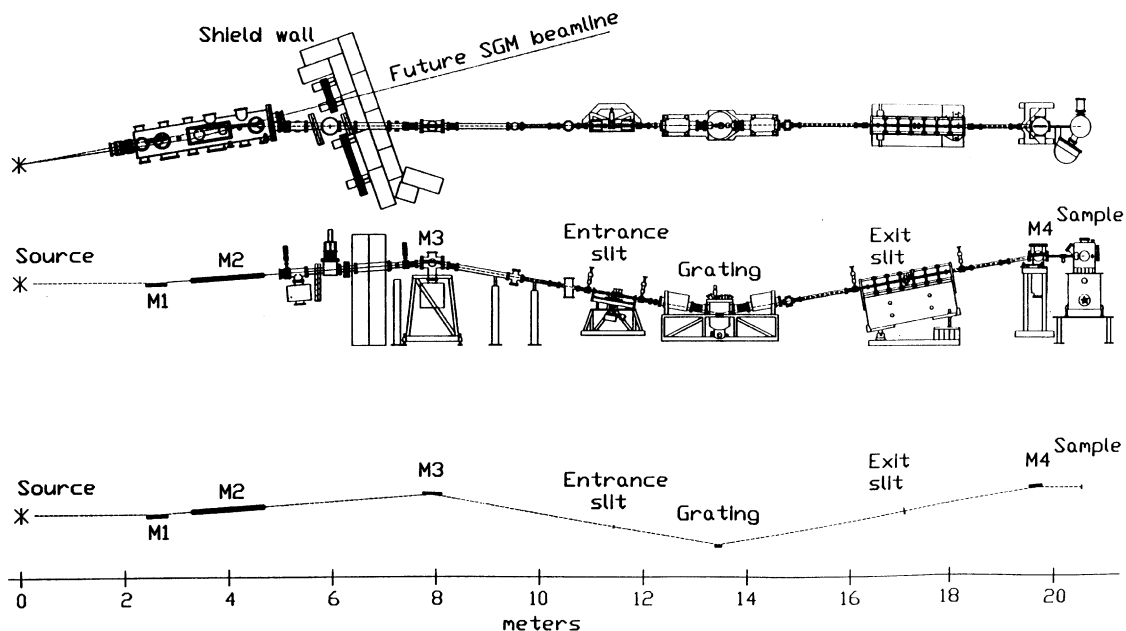


Fig. 1. Side view and plan view of CAMD 6-m TGM optical configuration showing primary optical elements.

Table 1
Optical elements of CAMD/TGM beamline^a

Optical element	Type	Cotaing, blank	Blank size W × L (mm)	Radius of curvature (mm)	Pole distance from source (mm)	Deflection angle (deg.)
M_1	Plane mirror	Gold, copper	80 × 400	—	2650	4
M_2	Bendable cylinder mirror	Gold, glass	20 × 1400	Variable	4050	10
M_3	Spherical mirror	Gold, copper	60 × 360	3995.73	8000	14
Entrance slit	Adjustrial jaws				11,500	—
G_1	Toroidal grating ~288 lines/mm					
G_2	Toroidal grating ~822 lines/mm	Gold, glass	45 × 125	$R=1924.6$	13,611	20
G_3	Toroidal grating ~2400 lines/mm			$r=47.05$		
Exit slit	Adjustrial jaws				17,500 (17,000–17,650)	—
M_4	Elliptical mirror	Gold, copper	40 × 250	$a=1600.0$	19,899	10
Target				$b=12.076$	20,699	—

^aSource paramter: $\sigma_v = 3.895 \times 10^{-7}$ rad cm, $\sigma_v = 2.9 \times 10^{-5}$ rad cm.

large mirror tank located behind the radiation wall. M_1 is a water-cooled copper plane mirror that deflects the beam upwards 4° and absorbs most (66% and 77% at 1.3 and 1.5 GeV, respectively) of the X-ray power. The 4° deflection also provides clearance for the front-end optics of the proposed SGM beamline. M_2 is a cylindrical mirror that accepts ~ 28 mrad of bending magnet radiation (source to M_2 pole is 4.05 m) and provides the horizontal focus. The mirror is based on a 4 cm high × 140 cm long piece of 1/4" thick float-glass. The mirror is mounted in a holder that permits adjusting its curvature as well as positioning its pole and orientation via stepper-motor-driven motion feedthroughs. The horizontal focus can be adjusted to occur at the entrance slit (7.45 m from the M_2 pole) or at any position further down the beamline thus permitting the use of spherical gratings.

The mirror M_3 is a spherical mirror that functions essentially as a cylindrical mirror to provide a vertical focus at the entrance slit. The source-to- M_3 distance is 8.00 m and the M_3 -to-entrance slit distance is 3.50 m yielding a vertical magnification of the synchrotron source of 0.43. M_3 is housed in a separate mirror tank outside the radiation shield and can be adjusted (roll, pitch, yaw) manually. The remainder of the beamline from entrance slit to the endstation utilizes the same optical and mechanical components installed

in the original TGM beamline at NSLS. The grating tank is a Physical Science Laboratory (PSL) design [5] with a 6-grating carousel. The variable position exit slit is mounted on linear bearings anchored to a granite block. The refocus mirror, M_4 , is an elliptical mirror that produces a 10° deflection and a nominal magnification (of the exit slit) of 0.33.

Fig. 2 displays ray tracing spot patterns that illustrate images of the source at the slits and beam filling factors at the various optical elements along the beamline. From these ray tracing results it is clear that the three-mirror front-end provides excellent coupling of 28 mrad of CAMD bending magnet radiation into the standard JY 6-m TGM. The maximum deflection angle in the system is 20° and occurs at the diffraction grating. The additional reflectance loss resulting from the three-element front end (compared to the single toroidal mirror front end) is more than compensated for by the larger collection angle; also, the three-element front end avoids the expense of a large water-cooled grazing angle-of-incidence toroid.

3. Construction details and initial M_2 evaluation

The scan drive, grating carousel, grating mounts and slit assemblies were constructed directly from

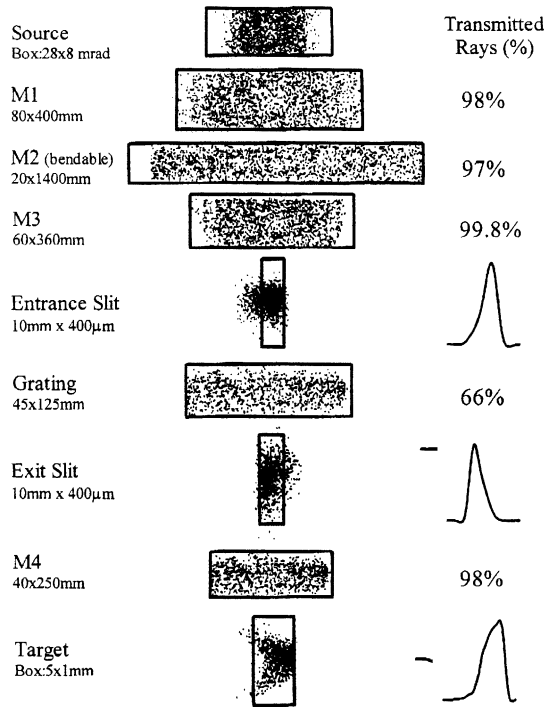


Fig. 2. Ray tracing spot patterns along 6-m TGM optical path: (a) mask (horizontal: 28 mrad); (b) M_1 plane mirror; (c) M_2 bent float-glass cylinder; (d) M_3 spherical mirror; (e) entrance slit; (f) grating; (g) exit slit; (h) M_4 elliptical mirror and (i) sample position. Source parameters and mirror parameters are given in text and Table 1.

drawings provided by PSL. This part of the TGM remains unchanged from the NSLS installation. The float-glass mirror mount was adapted from drawings, also provided by PSL, and mirror mounts for M_3 and M_4 were adapted from a design obtained from AT&T Bell Labs. The front-end optics for both the TGM (M_1 and M_2) and SGM (M_1) as well as the shutters for both beamlines and alignment diagnostics are integrated into a single large UHV mirror tank (~ 3 m in length pumped by two 400 l/s ion pumps) that serves as an optical table. Each beamline is serviced by a (in series) pair of water-cooled stepper-motor controlled shutters that permit a selection of masks to be placed in the radiation fan. The shutters are capable of modulating the polarization for magnetic circular dichroism measurements [6].

The float-glass bending jig [5] consists of a $4'' \times 1'' \times 55''$ bar of 304 stainless steel with a $2-1/2''$ wide channel milled out to clear the mirror. The mirror is supported near the four corners of its reflecting surface by four cylindrical posts and two fulcrums (on long arm levers) that extend across the mirror width at each end to provide bending torque. Care was taken to ensure that contact points of the four posts that support the mirror front surface are in a plane to avoid twisting the mirror along its major axis. The $55''$ long bar that serves as the mirror mount and carriage for the mirror-bending levers is kinematically mounted on a set of stepper-motor driven mechanical feedthroughs that provide the degrees-of-freedom to precisely position the mirror pole and perform pitch and roll angular adjustments. Two additional rotary motion feedthroughs coupled to the lever arm lead screws provide the capability to independently adjust the mirror radius upstream and downstream by moving the bending lever arm positions.

A sheet of selected $1/4''$ thick float-glass was purchased from Abrisa Industrial Glass [7] and cut into strips having dimensions suitable for the M_2 blank (51×1424 mm). Five of the float-glass mirror blanks were sent to the Advanced Photon Source (APS) Optical Metrology Lab at Argonne National Laboratory for evaluation by metrology techniques and subsequent thin-film coating. Optical surface roughness (using a WYKO-TOPO surface profile instrument) was measured on each of the five float-glass blanks. Several locations on each blank were measured and the best blank, having an average roughness RMS and peak-to-valley ($P-V$) of 0.29 and 3.2 nm, respectively, was selected for coating in the Deposition Laboratory at APS. The APS Optical Metrology Lab, using the same surface profilometry instrumentation measured the roughness of the coated mirror at nine locations. Average roughness values of 0.193 nm RMS and 0.99 nm $P-V$ were obtained. These average surface roughness values were surprisingly low and well within acceptable tolerances for the intended application.

Prior to installation in the beamline, a bench test of the M_2 bending jig mechanism was performed using a HeNe laser in combination with a

cylindrical lens. This source-lens combination provided an acceptably realistic approximation of the 28 mrad bending magnet source. In a 10° optical deflection geometry and with the cylindrical lens at a distance of 4.05 m from the M_2 pole (source M_2 distance), the mirror bending mechanism, via the mirror-bending levers, was adjusted to yield a horizontal focus at a distance of 7.45 m (M_2 -entrance slit distance). Optimum focusing was achieved by sequential small adjustments of the up- and down-stream mirror bending levers that adjust M_2 curvature. This *empirical* focusing procedure produced reproducible focused horizontal spot sizes of ~ 5 mm FWHM. The results of the bench test indicated that the M_2 bending jig mechanism would function as expected as an in situ adjustable optical element of the overall beamline.

Heat load estimates at M_1 and M_2 were carried out using SHADOW for 1.5 and 1.3 GeV ring energies. A maximum absorbed power density of $1.8 \text{ W/cm}^2/100 \text{ mA}$ is predicted along the center of M_1 at 1.5 GeV ring energy. With 1.5 GeV/170 mA operation, approximately 60 W of radiation is absorbed by M_1 and 30 W is transmitted to M_2 . A maximum absorbed power density of $0.35 \text{ W/cm}^2/100 \text{ mA}$ occurs along the center of M_2 , and at 1.5 GeV/170 mA, M_2 absorbs about 14 W. The maximum radiation flux at the entrance slit is approximately 15 W; approximately half of this power is reflected by the slits. No evidence of heat load related instabilities have been observed during the initial phase of beamline operation.

4. Theoretical performance estimates

The resolving power of the JY 6-m TGM grating set has been studied using ray tracing [2] based on holographic parameters provided by JY and analytically [4] based on a light path function model applied to a ruled toroid. The analytical treatment considered terms that describe the most important aberrations [6] including the defocusing and astigmatic coma. Slope errors in the toroidal grating were also considered in the analytical treatment. Fig. 3 compiles selected results of prior [2] and new ray tracing studies and analytical [4]

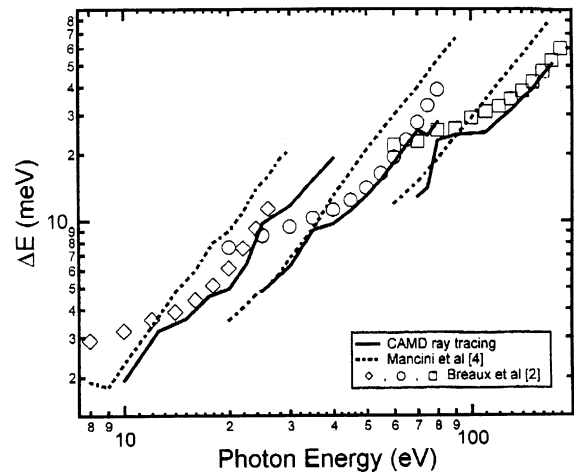


Fig. 3. Resolution (meV) vs. photon energy (eV) for the three JY toroidal gratings. All curves are based on exit slit position that optimizes resolution by reducing the defocus term in the instrument aberrations. Thick dashed lines, analytical results [4] based on light-path function analysis ($100 \times 100 \mu\text{m}$ slits with 0.5 arcsec slope errors); markers, ray tracing results [2] based on NSLS configuration; solid lines ray tracing results based on CAMD configuration.

studies of the 6-m TGM gratings. The Breau ray-tracing results [2], which optimized the NSLS beamline based on an astigmatic entrance slit focus, were repeated using the new CAMD front-end optics assuming a stigmatic (both vertical and horizontal) focus of the source at the entrance slit. All three studies indicate that when the exit slit is translated to minimize defocusing of the diffracted image, the ultimate theoretical resolving power, $E/\Delta E$, of all three gratings varies from approximately 5000 at the low-energy limit to about 1500 at the high-energy limit (assuming $100 \mu\text{m}$ slit settings). Slope errors in the grating figure of the order of 1 arcsec are predicted to significantly affect the resolution at slit settings of $25\text{--}50 \mu\text{m}$.

Theoretical estimates of bending magnet flux transmitted through the entrance slit and monochromatized flux at the sample were obtained using the SHADOW ray tracing program. These calculations were useful in judging the performance of the new front-end optics, including the float-glass mirror, and in judging the overall monochromator performance in comparison with measurements described later. Fig. 4 displays

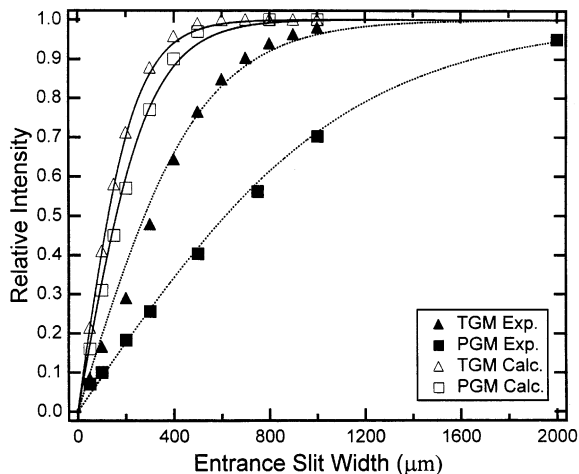


Fig. 4. Normalized measured flux through entrance slit (TGM and PGM) vs. entrance slit width. Theoretical flux through entrance slit (TGM and PGM [10]) vs. entrance slit width for source parameters in Table 1.

calculated and measured relative intensity of flux transmitted through the entrance slits of the TGM and a CAMD plane grating instrument that is discussed later. The calculated monochromatized flux at 0.1% bandwidth at 100 eV (200 μm slit settings) assuming a grating efficiency of 25% is 3×10^{13} photons/s at 170 mA ring current.

5. Optical alignment, tests and performance evaluation

The critical monochromator components (apertures, mirrors, slits and gratings) were located to an accuracy of about 1 mm (using plumb lines and measuring tapes) in relation to floor monuments referenced to the beam location within the storage ring. Minor adjustments of the optics [8,9] yielded zero order radiation footprints in agreement with ray tracing results (Fig. 2) indicating good first-order alignment. Initial tests based on Ar gas-phase photoemission and Fermi edge scans of a cold (30 K) metal surface indicated good energy resolution (better than 50 meV) and good flux from the low-energy grating. More quantitative measurements of the monochromatized flux based on a photodiode located at the target point (Fig. 5)

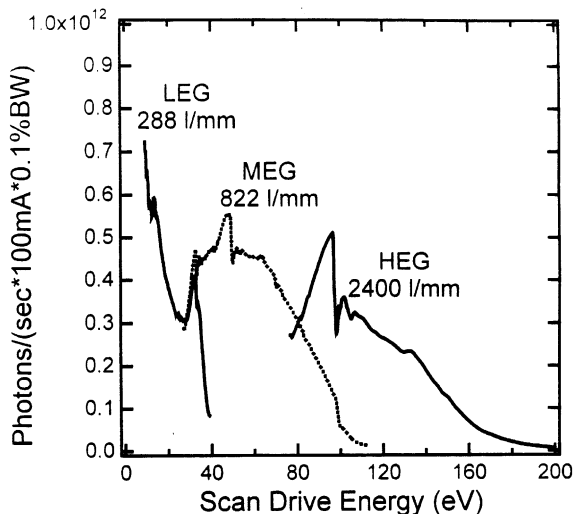


Fig. 5. Photon flux of LEG, MEG and HEG at the target point measured using a silicon diode—the spectra have been normalized to 0.1% BW and 100 mA ring current. Second-order light has not been eliminated and contributes to observed features due to better quantum efficiency for higher energy photons.

indicated a peak transmitted flux about an order of magnitude below the (optimistic) theoretical estimate of 3×10^{13} photons/s/0.1% bandwidth/170 mA. The wavelength response for all three gratings, including second-order flux, seemed reasonable suggesting that the flux loss resulted from either the float-glass mirror, or an overly optimistic representation of the source brightness in the ray-tracing exercise.

To determine if the float-glass mirror could be the cause of this loss in flux, a separate measurement was carried out on the CAMD McPherson plane grating monochromator (PGM) [10]. This beamline receives radiation from the same dipole magnet (port 4A, located right before the 6-m TGM). The optical elements of the PGM that focus the bending magnet radiation onto the entrance slit are high-quality mirrors [10] which are not expected to degrade the unity-magnification source image at the entrance slit. Note that the ratio of predicted-to-measured flux through the PGM entrance slit is approximately 0.3, which is comparable to the 0.4 ratio determined for the TGM. The ratio of measured TGM to PGM flux

at slit settings where the flux is increasing linearly is approximately equal to the ratio of the inverse of front-end magnification for the two beamlines which is 2.3 : 1.

Our interpretation of the results presented in Fig. 4 is that the effective CAMD bending magnet source size is considerably larger ($\approx 500\ \mu\text{m}$ compared to $100\ \mu\text{m}$) than the theoretical value used in the initial flux estimates. Consequently, we infer that the float-glass mirror does not contribute significantly to image distortion or subsequent associated loss of flux at the entrance slit. Non-statistical noise in high resolution photoemission spectra recently measured using the 6-m TGM suggest that a significant (and probably major) component of the reduced source brightness can be attributed to beam instabilities that can be corrected by a global beam stabilizing system.

Final grating adjustments, scan drive calibration and additional resolution tests were carried out using a resonance lamp (mounted just in front of the entrance slit) and a photodiode (mounted behind the exit slit). A helium discharge produces two narrow lines: He I $h\nu = 21.22\ \text{eV}$ and He II $h\nu = 40.81\ \text{eV}$. The angular spread of photons from the slit illuminated by the lamp capillary was sufficiently wide to uniformly illuminate the entire grating; in this sense the discharge lamp source can be assumed to simulate the bending magnet radiation that reaches the grating.

Fig. 6 displays a set of wavelength scans obtained using the low-energy grating (LEG) and He I radiation; the inset to Fig. 6 plots the corresponding resolution vs. exit slit width. Initially, to optimize the resolution of the helium lamp set-up, the exit arm length, r_b , was varied to optimize the resolution at the exit slit (for the discharge lamp using HeI, $r_b \sim 3550\ \text{mm}$). At this position the entrance slit was adjusted to $25\ \mu\text{m}$ width and the intensity behind the exit slit was measured for various exit slit widths as the monochromator was scanned. Next, the grating width was symmetrically masked yielding an effective area of about 25% of the grating surface (see Fig. 6). The energy resolution at $21.22\ \text{eV}$ photon energy and slit settings of $25 \times 50\ \mu\text{m}$ is seen to be about $7\ \text{meV}$. Removing the grating masks improved the flux by about a factor of four

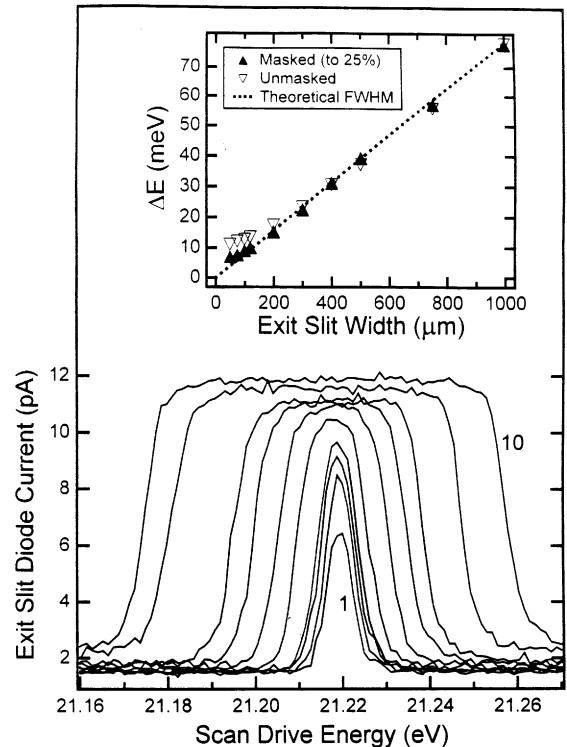


Fig. 6. Silicon diode current measured behind exit slit vs. scan drive energy for various exit slit widths (#1-10: 50, 75, 100, 120, 200, 300, 400, 500, 750, 1000 μm) obtained using the LEG and He I radiation incident at entrance slit set at $25\ \mu\text{m}$. Approximately 75% of the width of the grating was symmetrically masked. Inset: resolution vs. exit slit width for this data (as well as the unmasked data). The ultimate resolution ($7\ \text{meV}$) was reduced only slightly ($11\ \text{meV}$) for the unmasked grating.

while reducing the resolution to about $11\ \text{meV}$ (or resolving power of about 2000). The (approximately 40%) improvement in resolution resulting from masking the grating is consistent with Breaux's [2] ray tracing studies and suggests that astigmatic coma (and not surface figure errors) accounts for most of the loss in resolution when the full grating surface is illuminated. Breaux's analysis indicates that better resolution (and transmission) were obtained using an astigmatic focus at the entrance slit which focused a stripe of radiation on the grating surface. The float-glass M_2 permits placing the horizontal focus beyond the entrance slit. Additional studies may result in a higher transmission optical configuration that achieves $7\ \text{meV}$ resolution on the LEG.

Table 2
TGM calculated performance

Grating (lines/mm)	Photon energy (eV)	ΔE (meV) $100 \times 100 \mu\text{m}$ slits	r_b (mm)	Transmission (%) (0.1% BW)	Photon flux $\times 10^{12}/$ ($\text{s} \times 0.1\% \text{ BW} \times 100 \text{ mA}$)
288	10	1.9	3782	4.4	1.5
	15	3.6	3722	9.6	3.7
	20	4.9	3852	9.3	3.9
	25	9.7	4026	10.4	4.7
822	30	6.2	3756	7.6	3.6
	40	9.7	2709	14.6	7.5
	50	13.0	3777	15.9	8.7
	60	18.3	3885	11.7	6.7
	70	25.5	4008	12.9	7.8
2400	70	12.9	3935	6.8	4.1
	90	24.4	3741	13.2	8.4
	110	25.0	3703	20.6	13.9
	130	31.5	3730	22.5	15.7
	150	39.5	3790	16.4	11.7
	170	50.5	3865	6.1	4.5

Corresponding optimization and measurements, using He II ($h\nu = 40.81 \text{ eV}$) and the medium energy grating (MEG), produced similar curves with a resolving power of the order of 2000. It should be noted that the monochromator alignment with the discharge lamp provides a different source distribution at the entrance slit and footprint on the grating and this resulted in a different grating-to-slit distance for optimum resolution ($r_b \sim 3400 \text{ mm}$). As expected, the distance was closer to the values given with a partial filling of the grating by Breaux [2] ($r_b \sim 3522 \text{ mm}$).

Ray tracing calculations mentioned above for the optimized beamline performance required finding the best vertical focus at the exit slit. Our numerically calculated optimum exit arm lengths vs. photon energy are essentially identical to those calculated by Mancini [4] based on the analytical (light path function) method. Table 2 summarizes the calculated resolving power, transmitted flux and exit slit arm lengths that optimize the CAMD TGM performance.

6. Summary

A 6-m TGM has been installed and tested at the CAMD storage ring light source. A float-glass horizontal focusing element has been successfully

utilized in the front-end to couple 28 mrad of bending magnet radiation into the TGM. Ray tracing studies of the CAMD TGM optics confirm optimum coupling of the source to the JY grating set and establish optimum exit arm length settings. Close agreement between ray tracing optimization utilizing holographic grating parameters and corresponding light path function solutions based on a ruled toroid indicate that low-order aberrations (defocus and coma terms) are sufficient to characterize monochromator performance and that holographic corrections are not critical in the optimization process. Experiments carried out during commissioning established the CAMD source characteristics and verified the transmission and resolution properties of the TGM predicted by ray tracing.

Acknowledgements

The authors are pleased to acknowledge the useful assistance from the staff of Physical Sciences Laboratory (Stoughton, Wisconsin), the staff of APS Metrology Lab., the staff of CAMD and the excellent instrument making work of Allan Schroeder (UT Austin Machine Shop) who constructed the new components of the CAMD TGM including the water-cooled M_1 and shutter

assembly, M_2 bending jig and mounts, and the M_3 mirror tank. This work was supported by the Texas Higher Education Coordinating Board through technology and research grants ATP-171 and ARP-105, The RA Welch Foundation F-1015, and by NSF DMR 9972113.

References

- [1] Jobin Yvon Model Numbers: 2400/mm - 540.01.200 822/mm - 540.01 210; 288/mm—540.01.220.
- [2] L.H. Breaux, J.L. Erskine, Nucl. Instr. and Meth. A 246 (1986) 248.
- [3] C.T. Chen, E.W. Plummer, M.R. Howells, Nucl. Instr. and Meth. 222 (1984) 103.
- [4] D.C. Mancini, M. Bissen, D. Rioux, R. Patel, G. Rogers, E.L. Bradsy, H. Höchst, Rev. Sci. Instrum. 63 (1992) 1269.
- [5] The float-glass mirror mount, grating carousel, scan drive and slit assemblies were constructed based on designs provided by the Physical Sciences Laboratory, 3731 Schneider Drive, Stoughton, Wisconsin, 53589, USA.
- [6] W.R. McKinney, M.R. Howells, Nucl. Instr. and Meth. 172 (1980) 149.
- [7] Abrisa Industrial Glass, 1456 Fleet Ave., Ventura, California, 93003, USA.
- [8] D.J. Wallace, R.W.C. Hansen, F.K. Perkins, C.H. Pruett, J. Welnak, Nucl. Instr. and Meth. A 291 (1990) 231.
- [9] K-L. Tsang, P.-C. Tseng, C-I. Chen, Y-F. Song, S. Chung, T-E. Dann, H-F. Lin, L-R. Huang, C-N Chang, Rev. Sci. Instrum. 63 (1992) 1293.
- [10] E. Morikawa, J.D. Scott, E.D. Poliakoff, R.L. Stockbauer, V. Saile, Rev. Sci. Instrum. 63 (1992) 1300.